

Furrow-and-Ridge Morphology on Rockglaciers Explained by Gravity-Driven Buckle Folding: A Case Study From the Murtèl Rockglacier (Switzerland)

Marcel Frehner,^{1*} Anna Hui Mee Ling^{1,2†} and Isabelle Gärtner-Roer²

¹ Geological Institute, ETH Zurich, Zurich, Switzerland

² Department of Geography, University of Zurich, Zurich, Switzerland

ABSTRACT

Rockglaciers often feature a prominent furrow-and-ridge topography. Previous studies suggest that this morphology develops due to longitudinal compressive flow during rockglacier creep; however, no satisfactory mechanical/physical model has been provided explaining both the observed characteristic wavelength and the growth rate necessary to amplify the structure to its final size. Our study identifies viscous buckle folding as the dominant process forming the furrow-and-ridge morphology on rockglaciers. Buckle folding is the mechanical response of layered viscous media to layer-parallel compression.

The Murtèl rockglacier (Switzerland) exhibits a spectacular furrow-and-ridge morphology and is chosen as a case study. Its well-determined internal structure can be approximated by two layers: the upper 3–5 m thick active layer consisting mainly of rock boulders and fragments above a thick, almost pure, ice layer, both assumed to exhibit viscous rheology. We analysed a high-resolution digital elevation model of the Murtèl rockglacier using analytical buckle-folding expressions, which provide quantitative relationships between the observed wavelength, the layer thickness and the effective viscosity ratio between the folded layer and the underlying ice. Based on this geometrical and rheological information, we developed a finite-element model to simulate dynamical gravity-driven two-dimensional rockglacier flow. A buckling instability of the upper layer develops and amplifies self-consistently, reproducing several key features of the Murtèl rockglacier (wavelength, amplitude and distribution of the furrow-and-ridge morphology), as well as the quasi-parabolic deformation profile observed in boreholes. Comparing our model with published surface flow velocities constrains the time necessary to produce the furrow-and-ridge morphology to about 1000–1500 years. Copyright © 2014 John Wiley & Sons, Ltd.

KEY WORDS: rockglacier; furrow and ridge; morphology; buckle folding; finite element modelling; Murtèl

INTRODUCTION

Growing interest in rockglaciers paired with easy access via remote sensing techniques has led to an improved understanding of permafrost creep processes (Haeberli *et al.*, 2006, 2010). Despite a great variety in rockglacier morphology, their evolution and activity are often reflected in their shape and morphology.

Here, we follow Barsch (1992, p. 176) and define rockglaciers as 'lobate or tongue-shaped bodies of perennially frozen unconsolidated material supersaturated with

interstitial ice and ice lenses that move downslope or downvalley by creep as a consequence of the deformation of ice contained in them and which are, thus, features of cohesive flow'. This definition provides fundamental information on form, material and process, although knowledge of landform evolution and rheology is still limited. Rockglaciers are typically situated below steep rock faces or moraines, from where material is supplied to them. In the European Alps, they have typical lengths of 200–800 m and thicknesses of 20–100 m, as derived from direct coring or by geophysical sounding (Barsch, 1996). Morphological characteristics include steep lateral and frontal slopes at the angle of repose, with an apron of coarse blocks at the foot of the slope built by rockglacier creep. Often, several lobes are superimposed on top of each other, creating a complex topography from different rockglacier generations (Roer, 2007).

*Correspondence to: M. Frehner, Geological Institute /NO E3, ETH Zurich, Sonneggstrasse 5, 8092 Zurich, Switzerland.
E-mail: marcel.frehner@erdw.ethz.ch

†Present address: Rosenstiel School of Marine and Atmospheric Science, University of Miami, Miami, Florida, USA.

General rockglacier stratigraphy has been described by several authors (Haerberli, 1985; Barsch, 1992, 1996; Burger *et al.*, 1999; Humlum, 2000; Ikeda and Matsuoka, 2002) as a sequence of three main layers. The uppermost 1–5 m thick layer consists of large boulders and ridges. The second, underlying ice-rich permafrost layer comprises 50–70 per cent ice, fewer boulders and about 30–50 per cent finer-grained material (Barsch, 1996), which is creeping downslope. The third layer consists of larger blocks that were deposited at the rockglacier front and subsequently overrun by creeping permafrost. This characteristic sorting of rockglacier material is visible at the rockglacier front. More detailed studies on stratigraphy have been carried out by indirect means such as geophysical soundings (Vonder Mühl, 1993; Hauck *et al.*, 2001; Vonder Mühl *et al.*, 2001) or by direct observation in borehole cores (Vonder Mühl and Haerberli, 1990; Haerberli *et al.*, 1998; Arenson *et al.*, 2002).

Furrow-and-Ridge Morphology on Rockglaciers

The top layer of rockglaciers is typically composed of coarse (0.2–5 m) rock fragments and boulders (Humlum, 1998) and exhibits a 'surface relief' (Humlum, 1982) of ridges and furrows attributed to flow processes and indicating a complex history of rockglacier deformation (Haerberli, 1985; Johnson, 1992). A detailed description of 'microrelief on rock glaciers' is given in Wahrhaftig and Cox (1959). In general, such transverse ridges and furrows are thought to result from compressive flow (Haerberli, 1985; Käab *et al.*, 1998). Haerberli *et al.* (1998) describe longitudinal compression and vertical thickening in the lower part of the rockglacier as formative processes. However, they do not explain how the overall vertical thickening leads to the observed characteristic wavelength of the furrow-and-ridge structure; nor do they explain the localised thickening in the ridges. Field measurements and laboratory tests on the development of transverse ridges are discussed in Käab and Weber (2004). They conducted scaled analogue experiments in the laboratory, which generated characteristic furrow-and-ridge morphology. For both schematic interpretations put forward – bulging and thrusting – an explanation for the characteristic wavelength is missing. In addition, their scaled experiments comprise a homogeneous mixture of sand and water, yet their sketches show a layered medium. Consequently, their laboratory experiments do not fully explain the observed structures in rockglaciers. Springman *et al.* (2012) schematically explain rockglacier morphology by internal thrusts in the furrows leading to localised uplift in the ridges. In addition, they assume that the frontal part of a rockglacier acts as a buttress, resulting in longitudinal compression. Yet the characteristic wavelength remains unexplained. According to Wahrhaftig and Cox (1959) and Barsch (1977), variations in material supply may also lead to the formation of a complex surface topography.

Loewenherz *et al.* (1989) propose two mechanical models to explain the formation and characteristic wavelength of

rockglacier furrow-and-ridge morphology. The first model comprises a two-layer viscous medium flowing on a plane of constant slope. The layered nature of the medium leads to a flow instability if the upper layer exhibits higher viscosity than the underlying layer. This flow instability results in a surface morphology with a similar characteristic wavelength to that observed on rockglaciers. However, Loewenherz *et al.* (1989) argue that the growth rate of this instability is much too low to explain the natural furrow-and-ridge morphology. The second model comprises an elastic layer resting on a viscous layer. This composite medium is assumed to flow from a steeper plane to a shallower plane. The break in slope leads to layer-parallel compressive stresses in the elastic layer, which in turn lead to a buckling instability of the latter. The buckling instability exhibits a dominant wavelength similar to the characteristic wavelength of natural furrow-and-ridge morphologies. However, Loewenherz *et al.* (1989) admit that the elastic moduli of the upper layer are almost impossible to determine, which leads to a great uncertainty in their second model.

Even with the models of Loewenherz *et al.* (1989), the above interpretations for furrow-and-ridge development are schematic and no mechanical/physical explanation has been given. To overcome these limitations is the main motivation for this study. We combine the basic ideas of the two models of Loewenherz *et al.* (1989) by assuming a two-layer viscous model flowing on a plane with changing (decreasing) slope. The arising layer-parallel compressive stresses lead to viscous buckle folding. We identify viscous buckle folding as the main physical process for the formation of furrow-and-ridge morphology on rockglaciers, and apply a two-dimensional (2D) buckle-folding model to simulate the dynamic viscous rockglacier flow and reproduce realistic rockglacier topography. Results are compiled and discussed for the Murtèl rockglacier, where control data exist. Our overall aim is to elucidate rheological processes and their influence in shaping rockglacier topography.

Buckle Folding

Buckle folding is the response of a mechanically layered or stratified material to externally applied layer-parallel compression or shortening. Buckle folds are common structures in rocks (Ramsay and Huber, 1987) and have been studied extensively in the structural geology literature (reviewed by Hudleston and Treagus, 2010).

Here, we consider buckle folding of a viscous layer resting on a less viscous material. Various analytical expressions exist that provide relationships between the layer thickness, the viscosity ratio and the fold wavelength resulting from the buckling process. The seminal work of Biot (1961) and Ramberg (1963), which was restricted to 2D, infinitesimal amplitudes and large viscosity ratios, has later been extended to small viscosity ratios (Fletcher, 1974, 1977), to fully three-dimensional (3D) solutions

(Fletcher, 1991, 1995) and to finite amplitudes (Schmalholz and Podladchikov, 2000). The most complete analytical solution has been presented by Adamuszek *et al.* (2013) and captures buckle folding for both low viscosity ratios and up to large amplitudes.

All of these analytical studies indicate that buckle folding represents a wavelength selection process. Even though all wavelengths grow, one wavelength (the dominant wavelength) grows the fastest (Biot, 1961). At a finite amplitude stage, this wavelength selection process results in one wavelength that dominates the fold geometry, which is termed the preferred wavelength (Adamuszek *et al.*, 2013). We assume that wavelength selection during buckle folding is the reason for the characteristic wavelength of observed furrow-and-ridge morphology on rockglaciers. A very similar problem of surface folding of a layered viscous medium creeping downslope is encountered in the formation of pahoehoe lava. The characteristic wavelength in ropy pahoehoe lava has been described using the buckle-folding theory by Fink and Fletcher (1978) and Fink (1980).

STUDY SITE

Our test site is the Murtèl cirque, situated below the northern face of Piz Corvatsch (3300 m asl) in the Upper Engadin in southeastern Switzerland (at about 46°26'N/9°49'E). The site is a typical periglacial mountain slope with characteristic landforms: headwall, talus slopes or cones, and rockglaciers (Müller *et al.*, 2014). The entire slope, down to an altitude of 2620 m asl (rockglacier front), is situated in discontinuous permafrost (Gubler *et al.*, 2011). The lithology mainly consists of granodiorite, gneiss and schist. On account of easy accessibility the Murtèl cirque is one of the best-investigated permafrost sites and numerous data-sets (such as borehole temperatures and

deformations, ground surface temperatures and kinematics) are available (Hoelzle *et al.*, 2002).

As part of the Murtèl cirque, the Murtèl rockglacier (Figure 1) is particularly well suited for our investigation. It is probably one of the best-studied rockglaciers worldwide (e.g. Haeberli *et al.*, 2006; Springman *et al.*, 2012), and its surface geometry and internal structure are well documented. The structure can be approximated by a two-layer system: an upper layer consisting mainly of rock boulders and fragments (dynamical active layer), and a lower almost pure ice layer. For building a representative model, we require two key ingredients: (1) accurate geometrical information; and (2) information on the material rheology. Both ingredients are elucidated below.

DATA AND METHODS

Geometrical Information

To analyse the surface topography, we use a 1 m resolution digital elevation model (DEM; see Supplementary Information) based on low-altitude aerial photographs of the Swiss Permafrost Monitoring Network PERMOS (Gärtner-Roer, 2012). The 3D furrow-and-ridge morphology is evident when considering the differential digital elevation model (diffDEM; Figure 2), which is the true elevation minus the mean elevation within a diameter of 200 m at every point of the DEM. The same observation, but only in longitudinal topographic sections, was made by Käab *et al.* (1998) and Käab and Weber (2004). Applying a Fourier transform to longitudinal sections of the diffDEM indicates that the average wavelength of the furrow-and-ridge structure is around 20–25 m. The average amplitude is around 2 m.

Borehole deformation measurements (Wagner, 1992; Haeberli *et al.*, 1998; Arenson *et al.*, 2002), borehole image

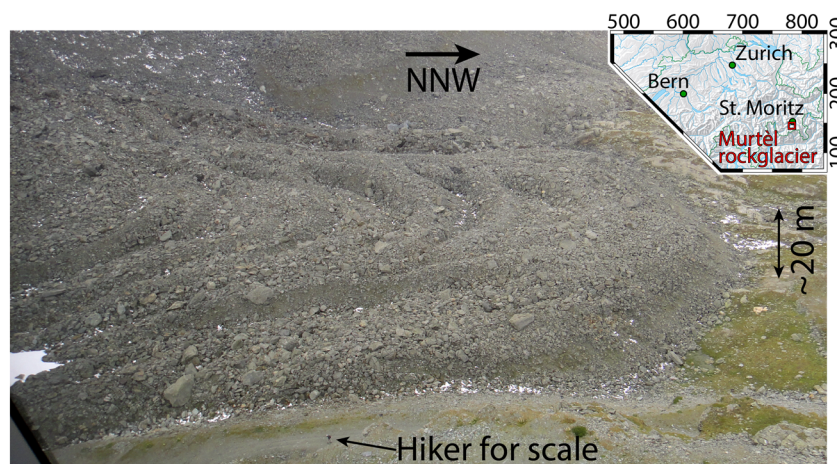


Figure 1 Photograph of the Murtèl rockglacier showing its surface furrow-and-ridge morphology. The photograph is taken out of the Murtèl-Corvatsch areal cableway. Inset: Map of Switzerland showing the location of the Murtèl rockglacier in the southeast (map from the Swiss Federal Office of Topography - swisstopo). Coordinates are given in the Swiss coordinate system CH1903. The exact coordinates of the Murtèl rockglacier are: 783'140/144'750. This figure is available in colour online at wileyonlinelibrary.com/journal/ppp

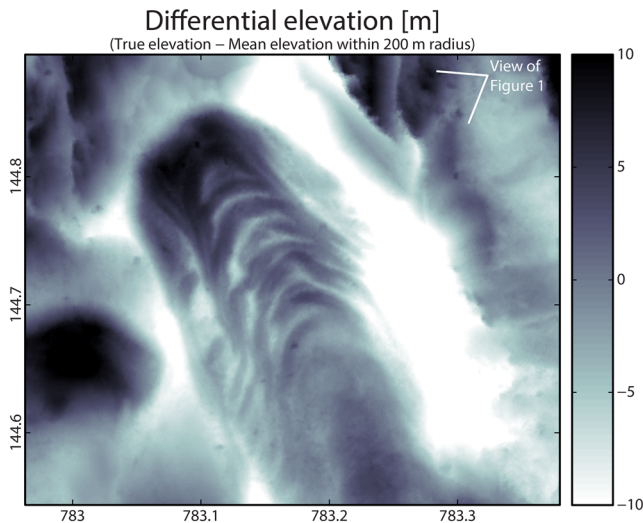


Figure 2 Differential digital elevation model (diffDEM) of the Murtèl rockglacier showing its surface furrow-and-ridge morphology. The diffDEM is calculated at every pixel as the true elevation minus the mean elevation within a circle of 200 m diameter. The employed 1 m resolution digital elevation model (DEM) is based on photogrammetry. Coordinates are given in the Swiss coordinate system CH1903. The DEM and the Matlab code to generate this figure are available in the Supplementary Information. This figure is available in colour online at wileyonlinelibrary.com/journal/ppp

logs (Arenson *et al.*, 2002) and the interpretation of integrated geoelectric, seismic and georadar data (Maurer and Hauck, 2007) demonstrate that the Murtèl rockglacier consists of four distinct layers. The active (topmost) layer freezes and thaws annually and is characterised by large rock fragments clearly visible at the rockglacier surface (Figure 1). It is 3–5 m thick; Kääh *et al.* (1998) speculated that the thickness of the active layer below ridges is larger than below furrows. The second layer (approx. 25 m thick), where the rockglacier flow takes place, is relatively homogeneous and consists of almost pure ice. The third layer, also comprising almost pure ice, corresponds to a 3 m thick shear zone (Arenson *et al.*, 2002). The lowermost layer is immobile and detached from the upper 30 m by the discrete shear zone.

Based on the available geometrical and geophysical information, we approximate the dynamic part of the Murtèl rockglacier as a two-layer system consisting of a lower 27 m thick ice-rich layer and an upper 3–5 m thick layer with large boulders, vent holes and less ice. Both layers are assumed to effectively obey a viscous flow law on the time-scale considered for the formation of the furrow-and-ridge morphology. The upper layer exhibits a higher effective viscosity because of its greater rock fragment content. The rockglacier below the shear zone at 30 m depth is not considered as important for the formation of furrows and ridges, since there is no movement, and is therefore neglected in our approach.

Rheological Information

Borehole deformation experiments (Wagner, 1992; Arenson *et al.*, 2002) demonstrate that the discrete shear zone at 30 m

depth accommodates approximately 60 per cent of the total deformation and the parabolic flow profiles above the shear zone can be approximated using a viscous flow law. Rheological studies (e.g. Glen, 1952; Nye, 1952) suggest that polycrystalline ice exhibits a power-law viscous rheology with a power-law exponent of about 3. However, for the upper layer it is impossible to determine the power-law exponent of an assumed effective viscous flow law because it is a complex mixture of ice and rock fragments and borehole deformation data in this layer are too sparse to infer rheology. Therefore, we treat both the lower almost pure ice layer and the upper layer as Newtonian (linear viscous) materials. This assumption also has the advantage that the modelled deformation does not depend on strain rate and the absolute values of viscosity, but only on the viscosity ratio between the two layers.

To determine the viscosity ratio, R , we assume that the furrow-and-ridge morphology is a result of viscous buckle folding of the upper layer. Existing buckle-folding theories provide relationships between observable geometrical parameters (e.g. wavelength, arc length, layer thickness, fold amplitude) and the viscosity ratio. The Fold Geometry Toolbox (FGT; Adamuszek *et al.*, 2011) is a specialised software that automatically analyses the geometry of a folded layer and applies various buckle-folding theories to determine the viscosity ratio, R , between the folded higher-viscosity layer and its surroundings. The FGT also estimates the bulk layer-parallel shortening, s , necessary to produce a given fold geometry (e.g. Schmalholz and Podladchikov, 2001). We inputted to the FGT longitudinal sections of the furrow-and-ridge geometry derived from the diffDEM (Figure 2; see Supplementary Information). We varied the thickness of the upper layer between 3 and 5 m (Figure 3A) according to its uncertainty and also used a non-constant thickness according to Kääh *et al.* (1998). The FGT calculations yielded viscosity ratios of $R = 9–21$, depending on the input model (Figure 3B). The bulk layer-parallel shortening is estimated as $s = 26–33$ per cent almost independently of the input model.

The upper layer is supported only from the bottom; it is not embedded in ice on both sides. In contrast, the buckle-folding theory of Schmalholz and Podladchikov (2001), which is implemented in the FGT, assumes a two-sided embedding. For a given wavelength and layer thickness, modified dominant wavelength expressions (Price and Cosgrove, 1990; Johnson and Fletcher, 1994) suggest that the viscosity ratio for one-sided support is half the viscosity ratio of a two-sided embedding. This correction is already included of factor 2 is already included in the estimated viscosity ratios for the Murtèl rockglacier (Figure 3B); hence, the relatively low viscosity ratios of $R = 9–21$ can be explained. In general, one-sided support of the folding layer also allows efficient buckle folding for lower viscosity ratios (Reber *et al.*, 2010).

Numerical Finite-Element Method and Model Setup

Based on this geometrical and rheological analysis, we designed a numerical finite-element (FE) model (Figure 4)

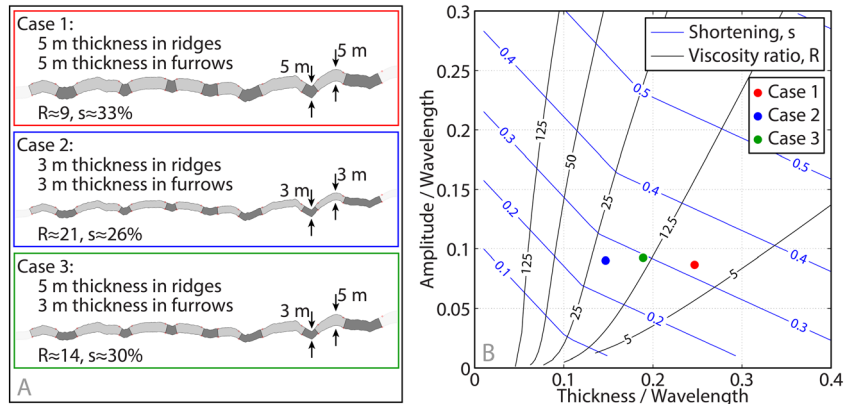


Figure 3 Geometrical and calculated rheological information of the Murtèl rockglacier. All sub-figures are modified screenshots from the Fold Geometry Toolbox (FGT) (Adamuszek *et al.*, 2011). (A) Three different input models for the upper layer of the rockglacier using different layer thicknesses in the furrows and ridges. Shades of grey indicate the furrows and ridges as identified by the FGT. (B) The resulting fold amplitude-to-wavelength- and thickness-to-wavelength-ratios with overlain shortening and viscosity ratio contour lines. The geometrical data that we used to generate this figure (derived from the diifDEM; Figure 2) can be found in the Supplementary Information. This figure is available in colour online at wileyonlinelibrary.com/journal/ppp

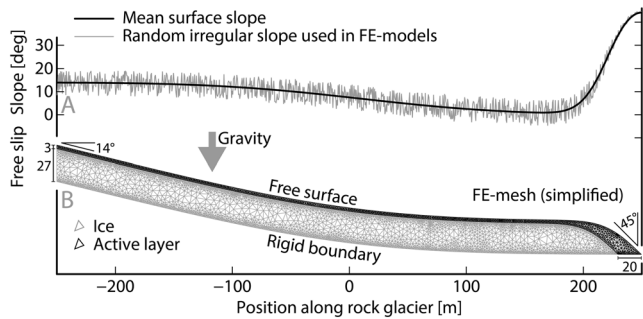


Figure 4 Initial model setup and boundary conditions of the employed finite-element (FE) model. The initial surface slope (A), the internal two-layer structure and the thickness of the two layers (values in metres in B) are inspired by the Murtèl rockglacier. The shown numerical triangular mesh (B) is simplified because the real mesh used in the FE simulations is too dense to be depicted here.

to simulate dynamic viscous rockglacier flow. The model solves the governing force-balance and rheological (Newtonian) equations in two dimensions. For the Murtèl rockglacier, the 2D approximation is justified because of its straight tongue-like geometry and unidirectional flow field (Kääb *et al.*, 1998). Details of the numerical technique can be found in Frehner and Schmalholz (2006); Frehner (2011) and Frehner *et al.* (2012), who all applied variations of this model to simulate viscous buckle folding under kinematic layer-parallel forcing. In the present model, the rockglacier flows solely under the effect of gravity.

The geometrical model setup is inspired by the Murtèl rockglacier geometry. However, our aim is not to simulate the development of the Murtèl rockglacier perfectly, but rather to test the feasibility of viscous buckle folding in explaining the first-order features observed on the rockglacier.

The model (Figure 4B) comprises two layers, a lower 27 m thick layer with lower viscosity and an upper 3 m thick

layer with a viscosity ratio of $R=21$. The density of the lower layer is 917 kg/m^3 (density of ice); the density of the upper layer (i.e., rock boulders and fragments) is 2000 kg/m^3 . The entire model is curved concave upwards, with a maximum basal slope at the back of the rockglacier of 14° and a minimum basal slope at the rockglacier front of close to 0° . The rockglacier surface is parallel to the base except for the front, where the surface slope reaches a maximum value of 45° , reducing the rockglacier thickness to zero. The entire length of the model is 500 m. The base of the rockglacier at 30 m depth is fixed, representing the transition to the immobile part. The free-slip boundary condition at the back of the model allows for traction-free vertical movement but prohibits horizontal movement; hence, this boundary does not allow new rockglacier material to flow into the model. This assumption is justified because the main area of furrow-and-ridge formation is much further down, at the rockglacier toe. The initial model surface is randomly disturbed (Figure 4A), representing natural irregularities of rock fragments and boulders, but also allowing the mechanical buckling instability to initialise. These initial irregularities correspond to a random red noise with a mean amplitude of 0.05 times the layer thickness of the upper layer.

RESULTS

Figures 5 and 6A show the initial state of the numerical FE model. Because we do not consider absolute viscosity values but only the viscosity ratio, the resulting horizontal normal stresses are normalised and cannot be interpreted as absolute stress levels. The upper layer exhibits layer-parallel compressive stresses (positive values) towards the toe of the rockglacier, which is also reflected by the orientation of the most compressive normal stress parallel to the

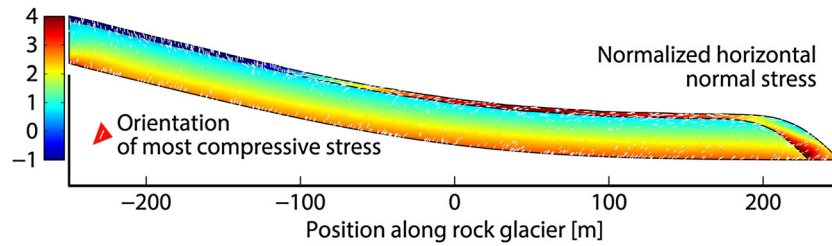


Figure 5 Normalised horizontal normal stress after one time step of the numerical FE simulation together with the orientation of the most compressive normal stress as white lines. This simulation snapshot represents the initial state of the model. Positive values represent compressive stresses. The scale of the x- and y-axis are equal. This figure is available in colour online at wileyonlinelibrary.com/journal/ppp

upper layer (white lines in Figures 5 and 6A). The almost pure ice layer immediately below the upper layer exhibits much smaller, but still layer-parallel compressive normal stresses. It is this discontinuous stress distribution across the layer interface that drives the mechanical buckling instability. In the upper part of the rockglacier, the upper layer exhibits layer-parallel tensile normal stresses (negative values). However, this region is influenced by the free-slip boundary condition, which prohibits the inflow of new rockglacier material.

For further analysis of the dynamic deformation, we focus on the rockglacier toe (Figure 6; see Supplementary Information – movie), where active buckle folding takes place during flow. Around 150 m uphill from the rockglacier front, the compressive normal stresses in the upper layer are largest; hence, buckle folds develop the fastest. Closer to the rockglacier front, buckle folds still develop, but at a lower rate. This is directly comparable to the furrow-and-ridge morphology on the Murtèl rockglacier (Figure 2), which exhibits the largest fold amplitudes around 150 m uphill from the rockglacier front. Generally, the amplification of buckle folds leads to a reduction of the compressive normal stresses in the upper layer (Figure 6), corresponding to a bulk softening of

the system (Schmalholz *et al.*, 2005). At the same time, the compressive normal stresses are redistributed during buckling, from vertically constant throughout the upper layer (Figure 6A) to increased inner-arc and decreased outer-arc compression, respectively (Figure 6C; Frehner, 2011). The modelled buckle folds develop self-consistently with a wavelength of around 20–25 m (Figure 6C), which is also directly comparable to the furrow-and-ridge morphology on the Murtèl rockglacier. The amplitudes in Figure 6C are comparable to the amplitudes observed today on the Murtèl rockglacier of about 2 m; hence, Figure 6C represents today's situation while Figure 6B represents an earlier situation, when the furrow-and-ridge morphology exhibits smaller amplitudes.

We also analyse modelled borehole deformation at three different locations similar to the boreholes on the Murtèl rockglacier about 150 m uphill from the rockglacier front (Wagner, 1992; Haerberli *et al.*, 1998; Arenson *et al.*, 2002). Figure 7 shows the modelled borehole deformation (coloured lines) from the surface down to the fixed model bottom. The different vertical deformations depend on whether a borehole is located on a ridge or in a furrow, which is not known when we place the boreholes at the

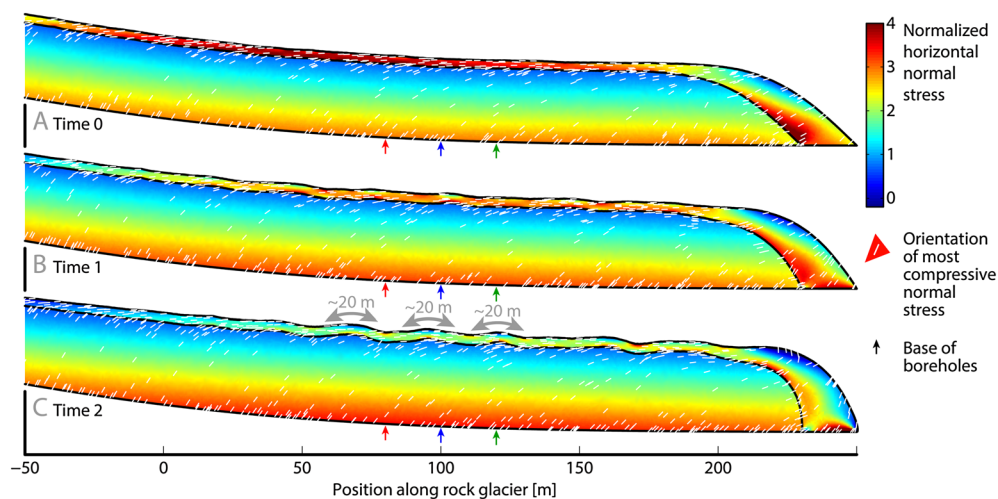


Figure 6 (A–C) Snapshots at three different times (Times 0–2) of the frontal part of the simulated rockglacier. Colours represent the normalised horizontal normal stress; white lines represent the orientation of the most compressive normal stress. The scale of the x- and y-axis are equal. Figure 6A corresponds to the initial state and is a zoom of Figure 5. Figure 6 is available as a movie in different file formats in the Supplementary Information. This figure is available in colour online at wileyonlinelibrary.com/journal/ppp

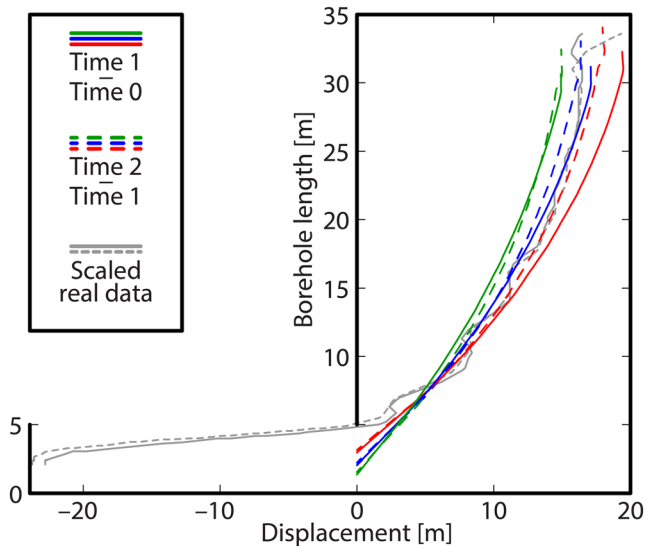


Figure 7 Modelled borehole deformation (coloured lines) between Times 0 and 1 and between Times 1 and 2 at three different locations indicated in Figure 6. The two grey lines correspond to borehole deformation data of Arenson *et al.* (2002) measured on the Murtèl rockglacier around 150 m uphill from the rockglacier front between November 1987 and March 1992 (solid line) and between November 1987 and August 1995 (dashed line). Both real deformation data sets are horizontally scaled to match the upper ~25 m of the numerical simulation. This figure is available in colour online at wileyonlinelibrary.com/journal/ppp

beginning of the simulation. The horizontal deformation of all boreholes and for both time intervals (Time 0–1 and Time 1–2) exhibits the typical parabolic shape, confirming the viscous flow profile within the rockglacier. The developing buckle folds disturb this otherwise smooth deformation profile at the transition to and within the upper layer. We compare the modelled borehole deformation with measured data from the Murtèl rockglacier (grey lines; Arenson *et al.*, 2002) from the surface down to the bottom of the shear zone. The measured data are scaled to match the upper ~25 m of the simulated borehole deformation. In general, the upper ~25 m of the real borehole deformation curves show, particularly in the uppermost 5 m, more variation and irregularity than the modelled curves. However, the modelled parabolic flow profiles approximate well the measured profiles. Hence, the modelled borehole deformation profiles can be directly compared to the real data in the upper ~25 m of the Murtèl rockglacier.

The simulated borehole deformation data do not reproduce the deformation in the basal shear zone (bottom ~5 m in Figure 7), where a large part of the deformation in the Murtèl rockglacier takes place. On account of matching of the upper ~25 m, the scaled real data exhibit negative displacement values in the shear zone.

DISCUSSION

The two models proposed by Loewenherz *et al.* (1989) served as a starting point for our investigation. We

adopted the two-layer viscous medium from their first model, and the changing slope from their second model but we did not assume an elastic layer. For the timescale and amount of deformation, rockglacier flow is dominated by viscous processes. Therefore, the elastic moduli of the active layer are not only challenging to assess, as Loewenherz *et al.* (1989) admit, but elastic deformation can be neglected entirely. At the same time, a decreasing slope induces layer-parallel compressive normal stresses in the upper layer (Figures 5 and 6). The resulting viscous buckle-folding process enhances the viscous flow instabilities on a constant slope suggested by Loewenherz *et al.* (1989), leading to more realistic growth rates of these instabilities.

The initial model setup of our numerical simulation represents a full-sized rockglacier without any surface morphology. In nature, such a situation will never occur as the furrow-and-ridge morphology already starts to develop during rockglacier advance. We chose this initial model setup as a simplified test case to reproduce several first-order features of the morphology and internal deformation of the Murtèl rockglacier. Our aim was not to accurately reproduce the entire rockglacier history.

Rheology

Naturally, our study exhibits limitations, mainly related to the rheological flow law. In nature, complex flow laws (e.g. power-law viscous or exponential flow laws) or even frictional rheological laws govern the localised deformation in the shear zone. Such complex rheology may be due to the presence of flowing water or grain-to-grain frictional contacts (Arenson *et al.*, 2002). The chosen Newtonian rheology does not accurately capture this deformation in the shear zone. Instead, the fixed lower boundary of our numerical model prevents the rockglacier front from advancing. As a consequence, the downslope flow leads to a vertical thickening of the frontal part of the rockglacier. Both this vertical thickening and the non-advancing rockglacier front contradict observed deformation patterns of the Murtèl rockglacier (Kääb *et al.*, 1998). However, the deformation above the shear zone is very well captured by the Newtonian flow law (upper ~25 m in Figure 7). Since the flow in this upper part of the rockglacier drives the formation of the furrow-and-ridge morphology, our study is useful in understanding processes, even though it does not accurately describe the shear zone.

A second limitation of the chosen Newtonian rheology is its incompressibility (i.e. volume-conserving formulation). In nature, volume change is mainly due to melting of the ice within the rockglacier. Even though measured vertical displacements (Kääb *et al.*, 1998; Arenson *et al.*, 2002) suggest some volume decrease of the Murtèl rockglacier, measured horizontal displacements still dominate the flow field. This suggests that volume-changing processes do not significantly alter

rockglacier dynamics, validating our assumption of incompressibility.

The third limitation of our model is that it does not incorporate temperature-dependent viscosity. The surface velocity of typical alpine rockglaciers oscillates around a mean value through the course of a year due to temperature variations (Arenson *et al.*, 2002). Because this oscillation is almost perfectly sinusoidal, we can describe the total rockglacier deformation of one year using averaged mechanical properties. Hence, the estimated viscosity ratio of $R = 21$ used in our numerical simulation does not represent the true viscosity ratio at any given time of the year, but the annual average.

Timing of Furrow-and-Ridge Development

Because we do not accurately capture deformation in the shear zone, our numerical simulation only accounts for about 40 per cent of the total surface deformation (Figure 7; Arenson *et al.*, 2002). Borehole deformation data and calculated surface flow fields based on photogrammetry and terrestrial geodetic surveys yield horizontal surface velocities along the studied longitudinal section of the Murtèl rockglacier of 5 cm/a^{-1} (Kääb *et al.*, 1998), 6 cm/a^{-1} (Wagner, 1992; Arenson *et al.*, 2002; Müller *et al.*, 2014), up to 9 cm/a^{-1} (Arenson *et al.*, 2002) and $10\text{--}12 \text{ cm/a}^{-1}$ (Gärtner-Roer, 2012; Müller *et al.*, 2014). Because the average surface velocity has generally increased during recent decades (Arenson *et al.*, 2002; Müller *et al.*, 2014), we assume that the lower surface velocity estimates of $5\text{--}6 \text{ cm/a}^{-1}$ are more appropriate for explaining current observations. With 40 per cent of this horizontal surface velocity, $625\text{--}950$ years are necessary to reach the modelled surface displacement of $15\text{--}19 \text{ m}$ (Figure 7).

While the natural 3D deformation (compared to the modelled 2D deformation) may not have a large effect on the flow pattern and the geometry of the resulting deformation structures, it does influence the rate at which this deformation takes place. Similar to the borehole deformation data for the vertical flow profile, the curved furrow-and-ridge morphology on the Murtèl rockglacier (Figure 2) indicates a viscous flow pattern also in map view. This pattern suggests that the flow is slowed down by viscous drag from the sides of the rockglacier, which is comparable to channel flow with a free surface. By applying standard open-channel flow equations (e.g. Chanson, 2004), we estimate the flow velocity reduction in such a 3D flow pattern to about 35 per cent compared to our modelled 2D flow pattern. Hence, the time necessary for developing the furrow-and-ridge morphology estimated in the previous paragraph has to be extended to $960\text{--}1460$ years. In other words, Time 1 in Figure 6 corresponds to $480\text{--}730$ years and Time 2 corresponds to $960\text{--}1460$ years after the initial model setup without a furrow-and-ridge morphology (Time 0). This time estimate suggests that the Murtèl rockglacier, and possibly other rockglaciers exhibiting a similar furrow-and-ridge morphology, existed already prior to the Little Ice Age.

CONCLUSIONS

Using the Murtèl rockglacier as an example, our study identifies gravity-driven viscous buckle folding as the dominant process to explain the formation of the furrow-and-ridge morphology characteristic of many rockglaciers. Buckle folding requires two main ingredients: (1) mechanical layering of the system; and (2) layer-parallel compression. For rockglacier systems, the first is due to a changing ratio between ice and rock fragments. Although the Murtèl rockglacier can be approximated with an upper bouldery layer and a lower almost pure ice layer, more complex multi-layer systems may occur, for example, when a rockglacier consists of several overriding tongues. The second is due to the convex curvature of a rockglacier towards its toe. In the steeper upper parts, the rockglacier flows more rapidly due to gravity and slows down towards the flatter frontal parts. This slowdown leads to layer-parallel compression in the area of the largest curvature. If a rockglacier exhibits a constant slope or the curvature is concave, for example, when it flows over a topographic step, the formation of a furrow-and-ridge morphology is hindered or even inhibited.

Our dynamical gravity-driven buckle-folding model reproduces several first-order features of the Murtèl rockglacier:

- the amplitudes and wavelengths of the furrow-and-ridge morphology;
- the location of the largest-amplitude structures around 150 m from the rockglacier front and smaller-amplitude structures closer to the front;
- the parabolic flow profiles measured in boreholes.

We conclude that gravity-driven buckle folding is the dominant process for the formation of the furrow-and-ridge morphology. Other factors may influence this process (e.g. grain-to-grain friction, flowing water, temperature variations), but only to a second order. We estimate that the time necessary to develop a furrow-and-ridge morphology as observed today on the Murtèl rockglacier from an undisturbed smooth topography to be $1000\text{--}1500$ years. Hence, the Murtèl rockglacier, and other rockglaciers exhibiting a well-developed furrow-and-ridge morphology, probably existed already prior to the Little Ice Age.

ACKNOWLEDGEMENTS

Parts of this publication originate from the joint Master's thesis of A. H. M. Ling at the ETH Zurich and the University of Zurich. We acknowledge the scientific discussions with Wilfried Haeblerli and Jean-Pierre Burg. This work was supported by the ETH Zurich and the University of Zurich. We thank the reviewers for their constructive comments that helped to improve the manuscript, and thank Ross Purves for editing the English.

REFERENCES

- Adamuszek M, Schmid DW, Dabrowski M. 2011. Fold geometry toolbox – Automated determination of fold shape, shortening, and material properties. *Journal of Structural Geology* **33**: 1406–1416. DOI: 10.1016/j.jsg.2011.06.003
- Adamuszek M, Schmid DW, Dabrowski M. 2013. Theoretical analysis of large amplitude folding of a single viscous layer. *Journal of Structural Geology* **48**: 137–152. DOI: 10.1016/j.jsg.2012.11.006
- Arenson L, Hoelzle M, Springman S. 2002. Borehole deformation measurements and internal structure of some rock glaciers in Switzerland. *Permafrost and Periglacial Processes* **13**: 117–135. DOI: 10.1002/ppp.414
- Barsch D. 1977. Nature and importance of mass-wasting by rock glaciers in Alpine permafrost environments. *Earth Surface Processes* **2**: 231–245. DOI: 10.1002/esp.3290020213
- Barsch D. 1992. Permafrost creep and rockglaciers. *Permafrost and Periglacial Processes* **3**: 175–188. DOI: 10.1002/ppp.3430030303
- Barsch D. 1996. *Rockglaciers: Indicators for the Present and Former Geocology in High Mountain Environments*. Springer Verlag: Berlin.
- Biot MA. 1961. Theory of folding of stratified viscoelastic media and its implications in tectonics and orogenesis. *Geological Society of America Bulletin* **72**: 1595–1620. DOI: 10.1130/0016-7606(1961)72[1595:TOFOSV]2.0.CO;2
- Burger KC, Degenhardt JJ, Giardino JR. 1999. Engineering geomorphology of rock glaciers. *Geomorphology* **31**: 93–132. DOI: 10.1016/S0169-555X(99)00074-4
- Chanson H. 2004. *The Hydraulics of Open Channel Flow: An Introduction*, Second Edition. Elsevier Butterworth-Heinemann: Oxford.
- Fink J. 1980. Surface folding and viscosity of rhyolite flows. *Geology* **8**: 250–254. DOI: 10.1130/0091-7613(1980)8<250:SFAVOR>2.0.CO;2
- Fink JH, Fletcher RC. 1978. Ropy pahoehoe: Surface folding of a viscous fluid. *Journal of Volcanology and Geothermal Research* **4**: 151–170. DOI: 10.1016/0377-0273(78)90034-3
- Fletcher RC. 1974. Wavelength selection in the folding of a single layer with power-law rheology. *American Journal of Science* **274**: 1029–1043. DOI: 10.2475/ajs.274.9.1029
- Fletcher RC. 1977. Folding of a single viscous layer: Exact infinitesimal-amplitude solution. *Tectonophysics* **39**: 593–606. DOI: 10.1016/0040-1951(77)90155-X
- Fletcher RC. 1991. Three-dimensional folding of an embedded viscous layer in pure shear. *Journal of Structural Geology* **13**: 87–96. DOI: 10.1016/0191-8141(91)90103-P
- Fletcher RC. 1995. Three-dimensional folding and necking of a power-law layer: Are folds cylindrical, and, if so, do we understand why? *Tectonophysics* **247**: 65–83. DOI: 10.1016/0040-1951(95)00021-E
- Frehner M. 2011. The neutral lines in buckle folds. *Journal of Structural Geology* **33**: 1501–1508. DOI: 10.1016/j.jsg.2011.07.005
- Frehner M, Schmalholz SM. 2006. Numerical simulations of parasitic folding in multilayers. *Journal of Structural Geology* **28**: 1647–1657. DOI: 10.1016/j.jsg.2006.05.008
- Frehner M, Reif D, Grasemann B. 2012. Mechanical versus kinematical shortening reconstructions of the Zagros High Folded Zone (Kurdistan Region of Iraq). *Tectonics* **31**: TC3002. DOI: 10.1029/2011TC003010
- Gärtner-Roer I. 2012. Sediment transfer rates of two active rockglaciers in the Swiss Alps. *Geomorphology* **167–168**: 45–50. DOI: 10.1016/j.geomorph.2012.04.013
- Glen JW. 1952. Experiments on the deformation of ice. *Journal of Glaciology* **2**: 111–114.
- Gubler S, Fiddes J, Keller M, Gruber S. 2011. Scale-dependent measurement and analysis of ground surface temperature variability in alpine terrain. *The Cryosphere* **5**: 431–443. DOI: 10.5194/tc-5-431-2011
- Haeberli W. 1985. *Creep of mountain permafrost: Internal structure and flow of alpine rock glaciers*. Mitteilungen der VAW/ETH Zürich 77, Versuchsanstalt für Wasserbau, Hydrologie und Glaziologie (VAW): Zurich.
- Haeberli W, Hoelzle M, Kääh A, Keller F, Vonder Mühl D, Wagner S. 1998. Ten years after drilling through the permafrost of the active rockglacier Murtèl, eastern Swiss Alps: Answered questions and new perspectives. In *Permafrost Seventh International Conference, June 23–27, 1998, Proceedings*, Lewkowicz AG, Allard M (eds). Collection Nordicana 57. Centre d'études Nordiques, Université Laval: Québec; 403–410.
- Haeberli W, Hallet B, Arenson L, Elconin R, Humlum O, Kääh A, Kaufmann V, Ladanyi B, Matsuoka N, Springman S, Vonder Mühl D. 2006. Permafrost creep and rock glacier dynamics. *Permafrost and Periglacial Processes* **17**: 189–214. DOI: 10.1002/ppp.561
- Haeberli W, Nötzli J, Arenson L, Delaloye R, Gärtner-Roer I, Gruber S, Isaksen K, Kneisel C, Krautblatter M, Phillips M. 2010. Mountain permafrost: Development and challenges of a young research field. *Journal of Glaciology* **56**: 1043–1058. DOI: 10.3189/002214311796406121
- Hauck C, Guglielmin M, Isaksen K, Vonder Mühl D. 2001. Applicability of frequency-domain and time-domain electromagnetic methods for mountain permafrost studies. *Permafrost and Periglacial Processes* **12**: 39–52. DOI: 10.1002/ppp383
- Hoelzle M, Vonder Mühl DV, Haeberli W. 2002. Thirty years of permafrost research in the Corvatsch-Furtschellas area, Eastern Swiss Alps: A review. *Norsk Geografisk Tidsskrift – Norwegian Journal of Geography* **56**: 137–145. DOI: 10.1080/002919502760056468
- Hudleston PJ, Treagus SH. 2010. Information from folds: A review. *Journal of Structural Geology* **32**: 2042–2071. DOI: 10.1016/j.jsg.2010.08.011
- Humlum O. 1982. Rock glacier types on Disko, central West Greenland. *Geografisk Tidsskrift* **82**: 59–66
- Humlum O. 1998. Active layer thermal regime at three rock glaciers in Greenland. *Permafrost and Periglacial Processes* **8**: 383–408. DOI: 10.1002/(SICI)1099-1530(199710/12)8:4<383::AID-PPP265>3.3.CO;2-M
- Humlum O. 2000. The geomorphic significance of rock glaciers: Estimates of rock glacier debris volumes and headwall recession rates in West Greenland. *Geomorphology* **35**: 41–67. DOI: 10.1016/S0169-555X(00)00022-2
- Ikeda A, Matsuoka N. 2002. Degradation of talus-derived rock glaciers in the Upper Engadin, Swiss Alps. *Permafrost and Periglacial Processes* **13**: 145–161. DOI: 10.1002/ppp.413
- Johnson AM, Fletcher RC. 1994. *Folding of Viscous Layers: Mechanical Analysis and Interpretation of Structures in Deformed Rock*. Columbia University Press: New York.
- Johnson PG. 1992. Micro-relief on a rock glacier, Dalton Range, Yukon, Canada. *Permafrost and Periglacial Processes* **3**: 41–47. DOI: 10.1002/ppp.3430030106
- Kääh A, Weber M. 2004. Development of transverse ridges on rock glaciers: Field measurements and laboratory experiments. *Permafrost and Periglacial Processes* **15**: 379–391. DOI: 10.1002/ppp.506
- Kääh A, Gudmundsson GH, Hoelzle M. 1998. Surface deformation of creeping mountain permafrost. Photogrammetric investigations on rock glacier Murtèl, Swiss Alps. In *Permafrost Seventh International Conference, June 23–27, 1998, Proceedings*, Lewkowicz AG, Allard M (eds). Collection Nordicana 57. Centre d'études Nordiques, Université Laval: Québec; 531–537.

- Loewenherz DS, Lawrence CJ, Weaver RL. 1989. On the development of transverse ridges on rock glaciers. *Journal of Glaciology* **35**: 383–391.
- Maurer H, Hauck C. 2007. Geophysical imaging of alpine rock glaciers. *Journal of Glaciology* **53**: 110–120. DOI: 10.3189/172756507781833893
- Müller J, Gärtner-Roer I, Kenner R, Thee P, Morche D. 2014. Sediment storage and transfer on a periglacial mountain slope (Corvatsch, Switzerland). *Geomorphology* **218**: 35–44. DOI: 10.1016/j.geomorph.2013.12.002
- Nye JF. 1952. The mechanics of glacier flow. *Journal of Glaciology* **2**: 82–93.
- Price NJ, Cosgrove JW. 1990. *Analysis of geological structures*. Cambridge University Press: Cambridge.
- Ramberg H. 1963. Fluid dynamics of viscous buckling applicable to folding of layered rocks. *AAPG Bulletin* **47**: 484–505.
- Ramsay JG, Huber MI. 1987. *The Techniques of Modern Structural Geology, Volume 2: Folds and Fractures*. Academic Press: London.
- Reber JE, Schmalholz SM, Burg J-P. 2010. Stress orientation and fracturing during three-dimensional buckling: Numerical simulation and application to chocolate-tablet structures in folded turbidites, SW Portugal. *Tectonophysics* **493**: 187–195. DOI: 10.1016/j.tecto.2010.07.016
- Roer I. 2007. *Rockglacier kinematics in a high mountain geosystem*. Bonner Geographische Abhandlungen 117, Asgard-Verlag: St. Augustin.
- Schmalholz SM, Podladchikov YY. 2000. Finite amplitude folding: Transition from exponential to layer length controlled growth. *Earth and Planetary Science Letters* **179**: 363–377. DOI: 10.1016/S0012-821X(00)00116-3
- Schmalholz SM, Podladchikov YY. 2001. Strain and competence contrast estimation from fold shape. *Tectonophysics* **340**: 195–213. DOI: 10.1016/S0040-1951(01)00151-2
- Schmalholz SM, Podladchikov YY, Jamtveit B. 2005. Structural softening of the lithosphere. *Terra Nova* **17**: 66–72. DOI: 10.1111/j.1365-3121.2004.00585.x
- Springman SM, Arenson LU, Yamamoto Y, Maurer H, Kos A, Buchli T, Derungs G. 2012. Multidisciplinary investigations on three rock glaciers in the Swiss Alps: Legacies and future perspectives. *Geografiska Annaler: Series A, Physical Geography* **94**: 215–243. DOI: 10.1111/j.1468-0459.2012.00464.x
- Vonder Mühl D. 1993. *Geophysikalische Untersuchungen im Permafrost des Oberengadins*, Mitteilungen der VAW/ETH Zürich 122, Versuchsanstalt für Wasserbau, Hydrologie und Glaziologie (VAW): Zurich.
- Vonder Mühl D, Haeberli W. 1990. Thermal characteristics of the permafrost within an active rock glacier (Murtèl/Corvatsch, Grisons, Swiss Alps). *Journal of Glaciology* **36**: 151–158.
- Vonder Mühl D, Hauck C, Gubler H, McDonald R, Russill N. 2001. New geophysical methods of investigating the nature and distribution of mountain permafrost with special reference to radiometry techniques. *Permafrost and Periglacial Processes* **12**: 27–38. DOI: 10.1002/ppp.382
- Wagner S. 1992. Creep of alpine permafrost, investigated on the Murtel rock glacier. *Permafrost and Periglacial Processes* **3**: 157–162. DOI: 10.1002/ppp.3430030214
- Wahrhaftig C, Cox A. 1959. Rock glaciers in the Alaska Range. *Geological Society of America Bulletin* **70**: 383–436. DOI: 10.1130/0016-7606(1959)70[383:RGITAR]2.0.CO;2

SUPPORTING INFORMATION

Additional supporting information may be found in the online version of this article at the publisher's web site.